Experimental and Numerical Studies of Lean Duplex Stainless Steel Beams

M. Theofanous and L. Gardner

Abstract

Stainless steel is well suited to a range of engineering applications owing to its durability and favourable mechanical properties. The most widely used grades of stainless steel are from the austenitic family and typically contain around 18% chromium and 8-11% nickel – these grades have a relatively high initial material cost, due, in part, to their high nickel content, and a nominal yield strength (in the annealed condition) of around 220 N/mm^2. A new, low nickel grade of stainless steel (UNS 32101/EN 1.4162), commonly referred to as 'lean duplex', has been developed, that offers over two times the strength of the familiar austenitic grades and at approximately half the initial cost – this lean duplex stainless steel appears well suited to load-bearing applications in construction. This paper reports material and 3-point bending tests on lean duplex stainless steel hollow sections. The 3-point bending tests were replicated by finite element (FE) analysis and, upon validation of the numerical models, parametric studies were conducted to assess the effect of key parameters such as cross-section aspect ratio, cross-section slenderness and moment gradient on the strength and deformation capacity of lean duplex stainless steel beams. Based on both the experimental and numerical results, appropriate slenderness limits and design rules, suitable for incorporation into structural stainless steel design standards, have been proposed.

Keywords: Beams, Experiments, Finite element, Hollow section, Lean Duplex, Numerical modelling, Stainless steel, Structural testing.

1. Introduction

Stainless steel is gaining increasing usage in construction, particularly in exposed architectural applications and in situations where long-term durability is paramount, with the austenitic grades being the most commonly specified. However, despite offering superior in-service performance compared to structural carbon steel, the high initial material cost, coupled with price fluctuations, inhibit more widespread usage in structures. Both can be largely attributed to the high nickel content (8-11%) present in the common austenitic stainless steel alloys, which represents a large portion of the total material cost. Lean duplex stainless steel is a new grade (UNS 32101/EN 1.4162) of stainless steel, which contains only approximately 1.5% nickel [1, 2]. Its price is therefore less dependant on that of nickel, thereby significantly reducing both the initial material cost and cost fluctuation. Despite the low nickel content, lean duplex stainless steel displays a good combination of strength, corrosion resistance and fatigue resistance, together with adequate weldability [3]. Early structural applications of lean duplex stainless steel include two footbridges, namely the Likholefossen bridge in Norway and the Siena footbridge in Italy [4].

The structural performance of lean duplex stainless steel has been relatively unexplored owing to its recent introduction, and to date there has been a lack of experimental data. To assess its structural behaviour, a comprehensive laboratory testing programme on grade UNS 32101 (EN 1.4162) stainless steel square and rectangular hollow sections (SHS and RHS) has been conducted at Imperial College London, including tensile, compressive and corner material coupon tests, stub column tests, long column tests and beam tests. The chemical composition and the tensile properties of the coil material from which the specimens where formed, as given in the mill certificates, are presented in Tables 1 and 2, respectively. This paper focuses on the basic material characteristics and on the flexural response of cold-rolled lean duplex stainless steel SHS and RHS beams. The beam tests were replicated numerically by means of non-linear finite element (FE) analysis. Upon validation of the FE models, parametric studies were conducted and the effect of key parameters, including the cross-section aspect ratio, cross-section slenderness (i.e. the width to thickness ratio of the most slender constituent plate element) and moment gradient on both ultimate moment capacity and rotation capacity has been investigated.

Lean duplex stainless steel is not currently covered in structural design standards. It is the intent of this paper to investigate whether the structural behaviour of lean duplex stainless steel justifies the extension of the scope of the current structural design codes to include this new grade of stainless steel. The suitability of the codified slenderness limits and the accuracy of the effective width equations for slender elements employed in Eurocode 3: Part 1-4 [5], SEI/ASCE-8 [6] and AS/NZS 4673 [7] is assessed. Comparisons between American, Australian and European codified provisions and the proposals made by the authors previously [8] regarding the treatment of local buckling within the classification system as well as within the recently developed continuous strength method [9, 10] are made. Finally the ultimate moment capacity of lean duplex stainless steel SHS and RHS beams is compared with other commonly used stainless steel grades and the significant economic merits of lean duplex stainless steel are discussed.

2. Material testing

A series of tensile and compressive coupon tests were carried out in the Structures laboratory of the Department of Civil and Environmental Engineering at Imperial College London, to obtain the basic material stress-strain response of the lean duplex stainless steel specimens, which was subsequently utilised in numerical modelling and in the analysis of the member test results. All material was extracted from the same length of tubes as the beam specimens. The tests were conducted in an INSTRON 600 kN machine in accordance with [11]. A uniform strain rate of 0.0003 s^{-1} was used throughout all tensile and compressive coupon tests. Strain gauges were affixed at either side of the tested coupons at mid height. Load, cross-head displacement, strain and input voltage were all recorded at one second intervals using the data acquisitions system DATASCAN.

Four section sizes were tested in the present study - SHS 60×60×3, SHS 80×80×4, SHS 100×100×4 and RHS 80×40×4. One tensile flat (labelled TF) and one compressive flat (labelled CF) coupon were machined longitudinally from each of the four faces of each of the four cross-sections (apart from the 80×40×4 for which only two compressive coupons were extracted from the longer faces), resulting in a total of sixteen tensile and fourteen compressive flat coupons. All tensile flat coupons had nominal dimensions of 320×20 mm, while the respective nominal dimensions for the compressive coupons were 72×16 mm.

Buckling of the compressive coupons was prevented by means of a bracing jig [9]. It is well-known that work-hardening induced by the cold-forming process leads to significant strength enhancements in the corner regions of both carbon steel [12] and stainless steel [13, 14] cold-formed sections. In order to quantify these strength enhancements and to accurately account for them in subsequent FE modelling, one 320 mm long tensile corner coupon (labelled TC) was extracted from the curved portions of each of the cross-sections considered. Upon machining from the cross-sections, longitudinal curving of all coupon specimens was observed due to the release of the bending residual stresses locked in the cross-sections. No attempt was made to straighten the coupons by plastic deformation prior to testing and hence the obtained stress-strain characteristics inherently include the effect of bending residual stresses, which were reintroduced during gripping in the testing machine's jaws and upon application of light loads [15, 16]. Previous studies [14, 17] have indicated that the magnitude of membrane residual stresses in cold-formed members is small compared to bending residual stresses. Hence membrane residual stresses have not been measured and were not explicitly accounted for in the numerical investigation detailed later on.

The obtained material data for each specimen are given in Table 3, whereas the weighted average (based on face width) tensile and compressive material properties of each section are given in Tables 4 and 5 respectively. The face labelling convention used in Table 3 is explained in Fig. 1. The material parameters reported in Tables 3-5 are the Young's modulus E, the 0.2% and 1% proof stresses $\sigma_{0.2}$ and $\sigma_{1.0}$, respectively, the ultimate tensile stress σ_u, the plastic strain at fracture ε_f (based on elongation over the standard gauge length $5.65\sqrt{A}$, where A is the cross-sectional area of the coupon), and the strain hardening exponents n and $n'_{0.2,1.0}$ used in the compound Ramberg-Osgood material model [9, 18-20]. A comparison between the measured the 0.2% and 1% proof stresses with those given in the mill certificates for the coil material is presented in Table 6. It should be noted that the properties reported in the mill certificates (see Table 2) were derived from tensile tests, possibly performed at higher strain rates that were employed herein, on transverse coupons (i.e. oriented perpendicularly to the rolling direction) and hence strain rate and anisotropy inherently influence the comparisons displayed in Table 6. Furthermore, possible deviations regarding the strain rate to which the coupon tests were conducted may have also influenced the results. The enhanced strengths generally displayed by the coupons extracted from the complete cross-sections over those given by the mill certificates for the coil material relate largely to strain hardening

during the cold-forming production process [13]. The weighted average stress-strain curves for SHS 100×100×4 are depicted in Fig. 2 as a representative indication of the differences in stress-strain response displayed by tensile flat, compressive flat and tensile corner lean duplex stainless steel material.

3. Beam Tests

Three-point bending tests were conducted to obtain the basic flexural response characteristics of lean duplex stainless steel cross-sections and assess the applicability of American and European codified slenderness limits and effective width formulae. A total of eight 3-point bending tests (two repeated tests per cross-section labelled B1 and B2) were carried out. The beams had a total length of 1300 mm and were simply supported between rollers, which were placed 100 mm inward from each end of the beam and allowed axial displacement of the beams' ends, as depicted in Fig. 3, resulting in 1100 mm clear span between the centrelines of the supports. The rectangular hollow section –RHS 80×40×4– was tested about its major axis. In all cases, the face containing the weld was the bottom (tension) flange of the beam.

Prior to testing, careful measurements of the geometry of the specimens, including initial geometric imperfections were taken. Only local imperfections were considered, since the nature and proportions of the test specimens precluded lateral torsional buckling. Imperfection measurements were taken along the centreline of the faces of each nominal section size following the procedure employed by [17]. Similarly to previous studies [21, 22], imperfection measurements were made over the central half of the specimen to eliminate the effect of flaring at the ends of the members due to the release of residual stresses upon cutting to length. The measured cross-sectional geometry and the maximum measured local geometric imperfection are reported in Table 7, where L is the length between centrelines of supports, B is the outer width of the section, D is the outer depth of the section, t is the thickness, r_i is the average internal corner radius and w_0 is the maximum measured local imperfection, defined as the maximum deviation of the centreline of each face of the cross-section relative to its edges.

Wooden blocks were placed within the tubes at the loading point to prevent web crippling, and load was applied through a steel block of thickness 15 mm and width 30 mm. Local bearing failure was prevented at the support locations by inserting steel plates between the

specimens and the rollers as shown in Fig. 3, whilst a steel block of 100×60×25 was inserted between the crosshead and the specimens thus ensuring a gradual dispersion of the stresses into the section. A thin layer of grease was applied between the rollers and the steel plates to minimize friction. A displacement transducer was placed at mid-span to measure the vertical deflection, while two further displacement transducers were positioned at a distance of 50 mm either side of the support at each end of the specimens in order to determine the end rotation of the beams, as shown in Fig. 3. Strain gauges were also affixed to the top and bottom flanges of the beams at a distance of 50 mm from the mid-span to measure the strain at the extreme tensile and compressive fibres of the cross-sections. The applied loading rate, in terms of crosshead movement rate, was 3 mm/min. Load, strain, displacement and input voltage were all recorded at 2 second intervals using the data acquisition system DATASCAN. All key experimental results are summarised in Table 8, where the elastic and plastic moment capacities M_{el} and M_{pl} were calculated by multiplying the relevant section modulus with the weighted average tensile 0.2% proof stress $\sigma_{0.2}$ of the section, derived from tensile flat coupon tests. The rotation at mid-span was defined as the sum of the end rotations since, once into the plastic regime when rotation capacity is of primary interest, the observed deformation pattern involved significant localised rotations at mid-span (i.e. the assumed plastic hinge position) with only negligible deformation occurring in the remainder of the specimen. The rotation capacities R were evaluated according to Eq. 1

$$R = \frac{\theta_u}{\theta_{pl}} - 1 \tag{1}$$

in which θ_u is the total rotation at mid-span when the moment-rotation curve falls back below M_{pl} as obtained from the test results and θ_{pl} is the elastic part of the total rotation at mid-span when M_{pl} is reached on the ascending branch, defined as $\theta_{pl} = \frac{M_{pl}L}{2EI}$, where I is the second moment of area of the section. In some cases (80×80×4-B1, 80×40×4-B1 and 80×40×4-B2) the ultimate rotation capacity was not recorded due to excessive deformations, which necessitated the premature termination of the test before the falling branch of the moment-rotation curve reached the value of M_{pl}. For these cases, the maximum recorded rotation was used instead of θ_u and the corresponding rotation capacities R are noted in Table 8. The recorded mid-span moment-rotation responses of the tested beams are depicted in Fig. 4.

4. Numerical modelling

The experimental part of the research was supplemented by numerical studies using the general purpose finite element analysis package ABAQUS. Finite element (FE) simulations were developed with the aim to replicate the experimental results and assess the sensitivity of the models to variation in key parameters such as initial geometric imperfections, material properties and mesh density. Upon validation of the numerical models, parametric studies were carried out to expand the available structural performance data over a wider range of cross-sectional slendernesses and aspect ratios.

The reduced integration 4-noded doubly curved general-purpose shell element S4R with finite membrane strains [23] has been employed in the present study to simulate the structural behaviour of the lean duplex stainless steel beams; this element has been shown to perform well in similar studies concerning modelling of thin-walled metallic structures [21, 22]. As discussed later, the corner properties, as derived from the corner coupon tests, were assumed to extend up to a distance equal to two times the material thickness into the flat region of each face of the models on either side of the corners. Mesh convergence studies revealed that two elements were required to discretise each of these flat parts adjacent to the corners, in order to accurately capture the effect of corner strength enhancements on the structural behaviour of the beams. If a uniform mesh size within all flat parts of the models was to be maintained, an element size equal to the material thickness was required for all models. A coarser, non-uniform mesh was shown to yield results of similar accuracy but given the already low computational cost associated with the models with the finer mesh size, a uniform mesh was maintained. Three linear elements were employed to approximate the geometry of the curved corners, which were assumed to be circular arcs.

The symmetry in geometry, boundary conditions, loading and failure modes exhibited by the tested specimens, was exploited in the numerical study by modelling only half the cross-section of each specimen considered and applying suitable symmetry boundary conditions along the assumed axis of symmetry. Even though half the length of the beams could have been modelled, the authors opted for modelling the full length, in order not to suppress possible antisymmetric local buckling modes, which, in some cases, had (marginally) lower corresponding eigenvalues than their symmetric counterparts. For modelling convenience, the

end cross-sections of the beams were constrained in-plane to remain undeformed, and appropriate degrees of freedom were restrained at the bottom flange to simulate simple support conditions. The load was applied as a point load at the junction of the web with the corner radius in the lower (tension) part of the beam to avoid web crippling.

Measured geometry and material properties as obtained from testing were incorporated into the models. The compound Ramberg-Osgood model, originally derived by [18] and further developed by [19] and [20] was adopted in the present study. The necessary material parameters have been determined and reported in Tables 3-5. As discussed earlier, cold-rolling leads to significant strength enhancements in the corner regions of cold-formed cross-sections; these strength enhancements extend beyond the curved corners into the flat regions. Due account of these enhancements in the FE simulation is necessary, if accurate results are to be obtained. Gardner and Nethercot [24] and Ashraf et al [25] concluded that accurate results are obtained if the strength enhancements of the corner regions are assumed to extend up to two times the thickness of the section considered beyond the corner regions for roll-formed sections. This conclusion was verified by later experiments [13] and this approach has been implemented in the present study. The tensile corner properties were assigned to the corner regions and to the flat parts extending to a distance of two times the thickness beyond the corners, while the weighted average tensile flat material properties (Table 4) were assigned to the flat tensile regions of the models (i.e. below the neutral axis) and the compressive flat material properties (Table 5) were assigned to the flat compressive regions of the models (i.e. above the neutral axis), as shown in Fig. 5. Residual stresses were not explicitly modelled since the experimentally obtained material properties inherently incorporate the effect of residual stresses, as discussed earlier.

For each set of material properties considered, the continuous engineering stress-strain curve defined by the compound Ramberg-Osgood model was initially approximated with a piecewise linear curve, the points of which were distributed such that the their density was proportional to the curvature of the continuous curve in order to obtain an optimal fit for a given number of discretisation points [26], following the procedure described by [22].

Geometric imperfections (i.e. deviations of the actual member geometry from the idealised one) are present in all structural members and affect their structural response. Due to the absence of global (member) buckling only local geometric imperfections have been

incorporated in the FE models in the form of the lowest buckling mode shape. A linear eigenvalue buckling analysis was therefore initially conducted using the subspace iteration method for eigenmode extraction. Subsequently a geometrically and materially non-linear analysis, incorporating geometric imperfections was carried out. The modified Riks method, which is essentially a variation of the classical arc-length method, was employed in the non-linear analyses to allow tracing of the post-ultimate path and hence the full load-deformation response of the models.

Four values of local imperfection amplitude were considered in the non-linear analyses. These were the maximum measured imperfection stated in Table 7, 1/10 and 1/100 of the cross-sectional thickness and the imperfection amplitude derived from the predictive model of Dawson and Walker [27] as adapted by Gardner and Nethercot [24] for stainless steels, which is defined by Eq. 2

$$w_0 = 0.023\left(\frac{\sigma_{0.2}}{\sigma_{cr}}\right)t \qquad (2)$$

In the calculations of the elastic buckling stress σ_{cr} of the plated elements, the flat plate width excluding the thickness of the adjoining elements and corner radii was used in conjunction with the buckling factors k_σ given in Eurocode 3: Part 1-5 [28]. For the $\sigma_{0.2}$, the average tensile flat 0.2% proof strengths given in Table 4 were used. Ideally, the constant multiplier in Eq. 4 is determined by regression analysis on available test data, however, due to the limited measured imperfection data for lean duplex stainless steel, the small plate slenderness range of the specimens considered in this research and the inherent scatter in geometric imperfection measurements, it was decided to adopt the value of 0.023 proposed by Gardner and Nethercot [24] for austenitic stainless steels.

The accuracy of the numerical results was assessed by comparing the maximum moment M_u and the corresponding rotation at maximum moment θ_m at the plastic hinge location (defined as the sum of the end rotations of the beam) with the respective test values. The full moment-rotation curves and the mode of failure were also compared. The results are tabulated in Table 9 for the various imperfection amplitudes considered. The incorporated imperfection amplitude can be seen to have only a modest effect on the ultimate moment capacity, whereas the rotation at ultimate moment seems to be more sensitive. In all cases, the initial stiffness,

failure mode and the general shape of the moment-rotation curves of the FE models closely matched those obtained from experiments. Overall, good agreement between experimental and numerical results can be observed, particularly in terms of the predicted ultimate moment capacity; the rotation at the plastic hinge is less accurately, but acceptably, predicted. A typical numerical and experimental failure mode (specimen 60×60×3-B2) is depicted in Fig. 6; both failure modes display local buckling in the compression flange and the upper part of the web. The corresponding experimental and numerical moment-rotation curves are depicted in Fig. 7.

Having validated the FE models against the test data, parametric studies were conducted to expand the available results over a wider cross-section slenderness range and investigate the effect of key factors, such as aspect ratio and moment gradient on the flexural response of lean duplex stainless steel beams. All modelled cross-sections had an overall depth D of 100 mm and an overall width B of either 100 mm or 50 mm thereby generating aspect ratios of 1.0 and 2.0 respectively. The thickness was varied between 0.82 mm and 3.25 mm for the 100×50 cross-sections and between 1.64 mm and 6.51 mm for the 100×100 cross-sections to provide a practical range of slenderness. For each cross-section considered, two beams with lengths of 1000 mm and 2000 mm were analysed in order to assess the effect of moment gradient on the rotation capacity of lean duplex stainless steel beams, which has been found to be quite significant in similar studies on carbon steel flexural members [29]. The material properties obtained from the coupon tests were used to define average material stress-strain curves for use in the parametric studies. Similarly to validation of the modes, the different material properties (tensile flat, tensile corner and compressive flat) were applied to the appropriate regions of the cross-section (see Fig. 5). The local geometric imperfections assumed the form of the lowest buckling mode shape and with an amplitude derived from Eq. 2. The generated numerical results are presented and discussed in the following section.

5. Analysis of results and design recommendations

5.1. Codified treatment of local buckling

The European structural stainless steel design Standard Eurocode 3: Part 1-4 [5] employs the concept of cross-section classification for the treatment of local buckling and assumes an

elastic-perfectly plastic material model for stainless steel as for carbon steel, with the 0.2% proof stress $\sigma_{0.2}$ being taken as the nominal yield stress. The plated elements that make up a structural cross-section are placed into one of four discrete behavioural classes by comparing their width-to-thickness ratios with specified slenderness limits. These slenderness limits depend on the element boundary conditions (i.e. internal or outstand referred to as stiffened and unstiffened respectively in the American Specification), the manufacturing process (whether cold-formed or welded) and the applied stress gradient; the cross-sectional response is assumed to relate to its most slender element. Class 4 cross-sections are characterised as slender and cannot reach their nominal yield stress $\sigma_{0.2}$ in compression – to reflect this, regions of the section rendered ineffective by local buckling are removed, and section properties are calculated on the basis of the remaining cross-section [5, 28]. Non-slender cross-sections in bending, which fail beyond the elastic moment capacity but prior to the attainment of the plastic moment capacity, are classified as Class 3 (fully effective), whereas they are Class 2 if the plastic moment capacity can be exceeded. Finally, cross-sections able to sustain their plastic moment capacities over large rotations and are hence suitable to be used in plastic design are deemed Class 1. It should be noted that plastic analysis and design is not permitted for structural stainless steel in EN 1993-1-4, despite the existence of a Class 1 limit. The classification approach for stainless steel [5] is similar to that adopted for carbon steel [30] with the only differences lying in the adopted slenderness limits and effective width formulae.

The American specification for the design of cold-formed stainless steel structural members, SEI/ASCE-8 [6], provides two alternative procedures for the determination of flexural capacity. The first procedure, which is similar to the European treatment for Class 3 and Class 4 cross-sections, is based on the initiation of yielding and assumes a linear stress distribution throughout the cross-section with the yield stress as the maximum allowable stress. A slenderness limit is given, beyond which loss of effectiveness occurs and an effective width formula applies. Unlike the European specification, which employs different effective width formulae for internal elements, cold-formed outstand elements and welded outstand elements, a single effective width formula for all plated elements is specified in SEI/ASCE-8 [6]. The second procedure utilises the inelastic reserve capacity brought about by the spread of plasticity through the section. This additional capacity may be exploited when certain criteria regarding web slenderness, shear stresses, cross-sectional geometry and the elimination of other possible modes of instability are met. The moment capacity is determined by integrating

an assumed stress distribution through the depth of the cross-section, accounting for possible loss of effectiveness by means of effective widths. The plastic moment capacity specified in EN 1993-1-4 [5] is an upper bound to the design resistance calculated with this method.

The Australian/New Zealand Design Specification for structural stainless steel AS/NZS 4673 [7] is similar to the SEI/ASCE-8 Specification [6], but with additional design provisions for tubular members. These provisions allow the attainment of a cross-sections' plastic moment resistance M_{pl}, provided that flange and web slendernesses conform to codified slenderness limits, similarly to EN 1993-1-4 [5].

5.2. Analysis of results and assessment of design provisions

In this section, the obtained test and FE results are compared with the current European and American design provisions to assess their applicability to lean duplex stainless steel flexural members. All comparisons have been carried out using measured geometry and material properties and with all safety factors set to unity. The second design procedure (based on inelastic reserve capacity) specified by SEI/ASCE-8 [6] and AS/NZS 4673 [7] has been used where applicable to obtain the flexural resistance.

Firstly, the suitability of the slenderness limits for fully effective (Class 3) sections is assessed. The moment capacity M_u obtained from the tests and FE analyses is normalised by the elastic moment capacity M_{el} and plotted against the slenderness parameter $c/t\varepsilon$ of the most slender constituent plate element of the section (which in all cases was the flange) in Fig. 8. The slenderness parameter $c/t\varepsilon$ is specified in Eurocode 3: Part-1-4, where c is the flat width of the plate element considered, t is the plate thickness and $\varepsilon = \sqrt{\frac{235}{\sigma_{0.2}} \frac{E}{210000}}$, $\sigma_{0.2}$ being the 0.2% proof stress and E being the Young's modulus. For internal simply supported elements (buckling factor k_σ=4) the following relationship between the European measure of slenderness $c/t\varepsilon$ and the slenderness parameter λ, specified in both the American and Australian standards [6, 7], holds:

$$\frac{c}{t\varepsilon} = 56.83\lambda \qquad (3)$$

The Class 3 limit specified in Eurocode 3: Part-1-4 is 30.7, whereas the equivalent Class 3 limit of the SEI/ASCE-8 [6] and AS/NZS 4673 [7] is 38.3. Recently, the authors [8] proposed the adoption of new slenderness limits within Eurocode 3: Part-1-4, which are based on all relevant published test data on stainless steel elements and have been statistically validated. The Class 3 limit proposed for internal elements in compression was 37, which is very close to the slenderness limit of 38.3 codified in [6, 7].

All three limiting slenderness values are plotted together with the test and FE results in Fig. 8. The SHS (D/B=1) may be seen to achieve higher normalised moment resistances than their RHS (D/B=2) counterparts with the same flange slenderness, particularly in the slender range of the graph. This is attributed to the lower web slenderness and the greater degree of restraint provided by the webs to the flanges, which delays the onset of local buckling, particularly for flanges of high slenderness, where failure occurs largely within the elastic material range. With decreasing slenderness, higher strains are achieved at ultimate moment and the stiffness is eroded by plasticity, which, in turn, reduces the restraint afforded to the flange. The moment gradient may be seen to have a minimal effect on moment capacity. Similar observations were made for carbon steel beams [29]. It can be concluded that the slenderness limit of 30.7 given in Eurocode 3: Part-1-4 [5] is overly conservative whereas the SEI/ASCE-8 [6] and AS/NZS 4673 [7] limit and that proposed by the authors [8] appear more suitable.
Figs. 9 and 10 compare the test and FE results with various moment capacity predictions for SHS (D/B=1) and RHS (D/B=2) respectively. In addition to the provisions of Eurocode 3: Part-1-4 [5], SEI/ASCE-8 [6] and, AS/NZS 4673, predictions of the flexural capacity based on the amendments to Eurocode 3: Part 1-4 proposed by the authors [8] and on the continuous strength method (CSM) are included. The CSM is a novel design method for structural stainless steel design, which is based on deformation capacity and utilises an accurate representation of the material response, allowing for stresses greater than the 0.2% proof stress to be achieved for stocky cross-sections [9, 11, 20, 31]. The relative accuracy of the four design approaches is displayed in Table 10. The CSM can be seen to most accurately predict the flexural capacity of the stainless steel beams, particularly in the stocky slenderness range, where stresses far beyond the 0.2% proof stress are reached. The SEI/ASCE-8 [6] and AS/NZS 4673 [7] predictions compare well with the test and FE results when the design procedure based on inelastic reserve capacity is applicable, whereas the procedure based on the initiation of yielding significantly underestimates the actual structural response of cross-sections with deep webs. The Eurocode 3: Part-1-4 [5] method offers good agreement with

the test and FE data in the slender range but is unduly conservative for stocky cross-sections due to the strict Class 3 limit adopted. Relaxing the Class 3 limit and effective width equations accordingly [8] improves accuracy, but failure to account for stresses higher than the 0.2% proof stress still compromises efficiency for stocky cross-sections.

The Class 2 slenderness limits (i.e. the limit below which the section's full plastic moment capacity can be attained) specified in [5] and [7] and the respective limit proposed by the authors is shown in Fig. 11, together with the test and FE results, where the ultimate moment has been normalised by the plastic moment capacity, defined as the plastic section modulus multiplied by the measured 0.2% proof strength. Similarly to Fig. 8, the section aspect ratio can be observed to have a marked influence on moment capacity, particularly for slender cross-sections. The Eurocode Class 2 slenderness limit of 26.7 may be seen to be rather conservative, whereas the Australian/New Zealand limit of 33.2 and the more relaxed limit of 35 proposed by the authors [8] seem more suitable.

The rotation capacity of both test and FE results, as defined in Eq. 1, is plotted against the flange slenderness in Fig. 12. Both aspect ratio and moment gradient may be seen to influence rotation capacity, with stockier webs and steeper moment gradients significantly enhancing the achievable rotation capacity. Neither the American nor the European Standards allow plastic analysis and design of stainless steel structures. Nonetheless a Class 1 limit of 25.7 is specified in Eurocode 3: Part 1-4. In Fig. 12, the rotation capacity requirement of R=3, adopted for carbon steel [32] and used as the basis for the Class 1 limit in Eurocode 3: Part 1-1 [30], is depicted assuming that this requirement is also applicable to stainless steel. The Class 1 limit of 33 proposed by the authors (which is the same limit that is applied to carbon steel in Eurocode 3: Part 1-1 [30]), judged on the basis of a rotation capacity requirement of R=3, appears unsafe for lean duplex stainless steel. However the actual material response of stainless steel significantly deviates from the bilinear elastic-perfectly plastic behaviour upon which the plastic design approach, based on concentrated plasticity in discrete plastic hinges, was originally derived. In fact, the gradual yielding of stainless steel and considerable strain hardening, together with the spread of plasticity throughout a plastic zone are believed to significantly reduce the ductility demands imposed on stainless steel structures for plastic design. There is a clear need for experimental data and research on the inelastic response of indeterminate stainless steel structures.

5.3. Comparison with other stainless steel grades

As outlined in the introduction, the low nickel content of lean duplex stainless steel leads to a more favourable initial material cost relative to the stainless steel grades commonly used in structural applications, namely the austenitic and duplex grades. The lean duplex stainless steel results reported in the present paper, together with austenitic and duplex stainless steel test data on SHS and RHS members subjected to 3-point and 4-point bending [33-37] have been utilised to assess the relative performance of the various stainless steel grades. The reported ultimate moment capacities from the tests have been normalised by the respective plastic section moduli and plotted against the c/t ratio of the compression flange of the sections in Fig. 13. Both the duplex and lean duplex stainless steel beams display superior moment capacity to their austenitic counterparts of similar flange slenderness, particularly for stocky sections, due to their higher 0.2% and 1% proof strengths. With a combination of superior structural performance and lower material cost, lean duplex appears well suited for wider use in structural applications.

6. Summary and conclusions

A series of material tests on tensile, compressive and corner coupons extracted from cold-formed lean duplex stainless steel SHS and RHS and eight major axis three-point bending tests have been reported in this paper. The obtained test data were used to develop FE models, upon the validation of which, parametric studies were conducted. Analysis of both experimental and numerical results allowed the effect of local slenderness, aspect ratio and moment gradient on both the load bearing and deformation capacity of lean duplex stainless steel SHS and RHS to be investigated and the suitability of the codified American [6], Australian/New Zealand [7] and European [5] provisions for lean duplex stainless steel flexural members to be assessed.

The current European Class 2 and Class 3 slenderness limits seem overly conservative for lean duplex stainless steel elements and the adoption of the more relaxed slenderness limits

proposed by the authors [8] is supported herein, which has already been shown to be suitable for other stainless steel grades. The current American and Australian/New Zealand design procedures have been shown to more accurately predict the ultimate moment capacity of lean duplex stainless steel SHS and RHS. Plastic design is not currently allowed in any design Standard for stainless steel; this topic requires further research. The recently proposed deformation-based design method for structural stainless steel cross-sections, termed the continuous strength method (CSM), has been found to provide better estimates of the ultimate moment resistance of lean duplex stainless steel than the American, Australian/New Zealand and European specifications. Overall, lean duplex stainless steel is shown to offer superior structural performance than the familiar austenitic grades and at a lower cost, making lean duplex stainless steel an attractive choice for structural applications.

Acknowledgements

The authors are grateful to Stalatube Finland for the supply of test specimens and to the Outokumpu Stainless Steel Research Foundation for project funding. They would also like to thank Gordon Herbert, Stéphanie Bouhala and Cheryl Parmar for their contribution to the experimental part of this research.

References

[1] ASTM Standard A240/A240M-09a. (2009). Standard Specification for Chromium and Chromium-Nickel Stainless Steel Plate, Sheet, and Strip for Pressure Vessels and for General Applications. ASTM International, West Conshohocken, PA.

[2] EN 10088-4. (2009) Stainless steels – Part 4: Technical delivery conditions for sheet/plate and strip of corrosion resisting steels for general purposes. CEN.

[3] Nilsson, J. O., Chai, G. and Kivisäkk, U. (2008). Recent development of stainless steels, Proceedings of the Sixth European Stainless steel Conference, pp. 585-590, Finland.

[4] Gedge, G. (2008). Structural uses of stainless steel — buildings and civil engineering. Journal of Constructional Steel Research, 64(11): 1194-1198.

[5] EN 1993-1-4. (2006) Eurocode 3: Design of steel structures - Part 1.4: General rules - Supplementary rules for stainless steel. CEN.

[6] American Society of Civil Engineers (ASCE). (2002). "Specification for the design of cold-formed stainless steel structural members." SEI/ASCE-8, ASCE, Reston, Va.

[7] AS/NZS 4673 (2001). Cold-formed stainless steel structures, AS/NZS4673, Standards Australia, Sydney.

[8] Gardner, L. and Theofanous, M. (2008). Discrete and continuous treatment of local buckling in stainless steel elements. Journal of Constructional Steel Research, 64(11): 1207-1216.

[9] Gardner, L. and Nethercot, D.A. (2004). Experiments on stainless steel hollow sections - Part 1: Material and cross-sectional behaviour. Journal of Constructional Steel Research. 60(9), 1291-1318.

[10] Ashraf, M., Gardner, L. and Nethercot, D. A. (2008). Structural stainless steel design: Resistance based on deformation capacity. Journal of Structural Engineering, ASCE. 134(3), 402-411.

[11] EN 10002-1 (2001). Metallic materials – Tensile testing – Part 1: Method of test at ambient temperature, CEN.

[12] Karren, K.W. (1967). Corner properties of cold-formed steel shapes. Journal of the Structural Division, ASCE. ST1, 401-432.

[13] Cruise, R.B. and Gardner, L. (2008). Strength enhancements induced during cold forming of stainless steel sections. Journal of Constructional Steel Research. 64 (11), 1310-1316.

[14] Young, B. and Lui, W.M. (2005). Behavior of cold-formed high strength stainless steel sections. Journal of Structural Engineering, 131 (11), 1738-1745.

[15] Rasmussen K.J.R. and Hancock G.J. (1993a). Design of cold-formed stainless steel tubular members. I: Columns. Journal of Structural Engineering, ASCE , 119(8), 2349-2367.

[16] Cruise, R.B. and Gardner, L. (2008). Residual stress analysis of structural stainless steel sections. Journal of Constructional Steel Research. 64(3), 352-366.

[17] Schafer, B.W. and Peköz, T. (1998). Computational modeling of cold-formed steel: characterizing geometric imperfections and residual stresses. Journal of Constructional Steel Research 47(3), 193-210.

[18] Mirambell, E. and Real, E. (2000). On the calculation of deflections in structural stainless steel beams: an experimental and numerical investigation. Journal of Constructional Steel Research. 54(1), 109-133.

[19] Rasmussen, K.J.R. (2003). Full-range stress-strain curves for stainless steel alloys. Journal of Constructional Steel Research. 59(1), 47-61.

[20] Gardner, L. and Ashraf, M. (2006). Structural design for non-linear metallic materials. Engineering Structures. 28(6), 926-934.

[21] Theofanous, M., Chan, T.M. and Gardner, L. (2009). Structural response of stainless steel oval hollow section compression members. Engineering Structures, 31(4): 922-934.

[22] Theofanous, M., Chan, T.M. and Gardner, L. (2009). Flexural behaviour of stainless steel oval hollow sections. Thin-walled Structures, 47(6-7): 776-787.

[23] Hibbitt, Karlsson & Sorensen, Inc (2006). ABAQUS. ABAQUS/Standard user's manual volumes I-III and ABAQUS CAE manual. Version 6.6. (Pawtucket, USA).

[24] Gardner, L. and Nethercot D.A. (2004). Numerical Modeling of Stainless Steel Structural Components-A Consistent Approach. Journal of Structural Engineering, ASCE. 130(10), 1586-1601.

[25] Ashraf, M., Gardner, L. and Nethercot, D.A. (2006). Finite element modelling of structural stainless steel cross-sections. Thin-walled structures 44(10), 1048-1062.

[26] Koltsakis, E.K. and Preftitsi, F.G. (2008). Numerical investigation of the plastic behaviour of short welded aluminium double-T beams. Engineering Structures 30 (7), 2022-2031.

[27] Dawson, R.G. and Walker, A.C. (1972). Post-buckling of geometrically imperfect plates. Journal of the Structural Division, ASCE. 98:ST1, 75-94.

[28] EN 1993-1-5 (2006) Eurocode 3. Design of Steel Structures: Part 1-5: Plated structural elements. CEN.

[29] Kuhlmann, U. (1989). Definition of Flange Slenderness Limits on the Basis of Rotation Capacity Values. Journal of Constructional Steel Research. 14(1), 21-40.

[30] EN 1993-1-1. (2005) Eurocode 3: Design of steel structures - Part 1.1: General rules – General rules and rules for buildings. CEN.

[31] Ashraf, M., Gardner, L. and Nethercot, D.A. (2006). Compression strength of stainless steel cross-sections. Journal of Constructional Steel Research, 62(1-2), 105-115.

[32] Sedlacek, G. and Feldmann, M. (1995). The b/t-ratios controlling the applicability of analysis models in Eurocode 3, Part 1.1. Background Document 5.09 for chapter 5 of Eurocode 3, Part 1.1, Aachen.

[33] Rasmussen, K.J.R. and Hancock, G.J. (1993). Design of cold-formed stainless steel tubular members II: Beams. Journal of Structural Engineering, ASCE, 119(8), 2368-2386.

[34] Talja, A. and Salmi, P. (1995). Design of stainless steel RHS beams, columns and beam-columns. Research note 1619. Finland: VTT Building Technology.

[35] Gardner L. and Nethercot D.A. (2004). Experiments on stainless steel hollow sections – Part 2: Member behaviour of columns and beams. Journal of Constructional Steel Research, 60(9), 1319-1332.

[36] Real, E. and Mirambell, E. (2005). Flexural behaviour of stainless steel beams. Engineering Structures, 27(10), 1465-1475.

[37] Zhou, F. and Young, B. (2005). Tests of cold-formed stainless steel tubular flexural members. Thin-Walled Structures, 43(9), 1325-1337.

Table 1: Chemical composition of grade EN 1.4162 stainless steel specimens

Section	C (%)	Si (%)	Mn (%)	P (%)	S (%)	Cr (%)	Ni (%)	N (%)	Mo (%)	Cu (%)
60×60×3	0.025	0.8	4.99	0.02	0.001	21.64	1.5	0.209	0.3	0.31
80×80×4 and 80×40×4	0.028	0.7	4.85	0.021	0.001	21.4	1.6	0.229	0.26	0.29
100×100×4	0.019	0.64	5.05	0.02	0.001	21.41	1.6	0.227	0.28	0.34

Table 2: Mechanical properties stated in mill certificates

Cross-section	$\sigma_{0.2,mill}$ (N/mm^2)	$\sigma_{1.0,mill}$ (N/mm^2)	$\sigma_{u,mill}$ (N/mm^2)	ε_f (%)
SHS 100×100×4	605	658	777	33
SHS 80×80×4	540	605	752	37
SHS 60×60×3	570	641	770	33
RHS 80×40×4	540	605	752	37

Table 3: Coupon test results for each specimen

Cross-section	Coupon-Face	E (N/mm^2)	$\sigma_{0.2}$ (N/mm^2)	$\sigma_{1.0}$ (N/mm^2)	σ_u (N/mm^2)	ε_f %	Compound R-O coefficients	
							n	$n'_{0.2,1.0}$
SHS 100×100×4	TF-1	198820	614	736	767	48	9.0	2.4
SHS 100×100×4	TF-2	200160	552	595	748	46	9.2	2.2
SHS 100×100×4	TF-3	200180	569	611	760	45	10.7	2.7
SHS 100×100×4	TF-4	195920	609	666	767	49	7.1	3.8
SHS 100×100×4	CF-1	197330	587	662	-	-	6.9	2.4
SHS 100×100×4	CF-2	196040	513	613	-	-	6.1	2.8
SHS 100×100×4	CF-3	197180	507	609	-	-	5.9	2.7
SHS 100×100×4	CF-4	202410	635	685	-	-	14.3	2.5
SHS 100×100×4	TC	206000	811	912	917	32	6.3	4.1
SHS 80×80×4	TF-1	191900	686	753	777	40	5.6	5.0
SHS 80×80×4	TF-2	199070	665	710	745	42	7.3	3.3
SHS 80×80×4	TF-3	201270	642	687	757	43	7.6	3.6
SHS 80×80×4	TF-4	207220	723	795	812	44	5.8	4.8
SHS 80×80×4	CF-1	195460	692	787	-	-	4.8	2.1
SHS 80×80×4	CF-2	197460	622	734	-	-	4.6	2.6
SHS 80×80×4	CF-3	201130	630	742	-	-	4.6	2.8
SHS 80×80×4	CF-4	194750	684	816	-	-	4.9	2.7
SHS 80×80×4	TC	210000	731	942	959	24	5.6	3.7
SHS 60×60×3	TF-1	230960	825	906	935	47	5.5	5.1
SHS 60×60×3	TF-2	208920	717	770	790	44	5.1	4.1
SHS 60×60×3	TF-3	211800	742	793	814	36	6.3	4.0
SHS 60×60×3	TF-4	187390	736	809	817	49	7.0	4.0
SHS 60×60×3	CF-1	204450	739	869	-	-	6.0	2.7
SHS 60×60×3	CF-2	219940	712	860	-	-	4.2	3.1
SHS 60×60×3	CF-3	195610	686	811	-	-	4.5	2.3
SHS 60×60×3	CF-4	206370	707	844	-	-	5.3	2.7
SHS 60×60×3	TC	212400	885	1024	1026	22	6.3	4.0
RHS 80×40×4	TF-1	196610	811	890	894	52	7.3	4.3
RHS 80×40×4	TF-2	200700	698	736	785	63	10.9	2.9
RHS 80×40×4	TF-3	199080	708	744	789	45	11.6	2.7
RHS 80×40×4	TF-4	200830	782	861	860	33	8.4	4.7
RHS 80×40×4	CF-1	-	-	-	-	-	-	-
RHS 80×40×4	CF-2	215270	576	714	-	-	4.4	2.9
RHS 80×40×4	CF-3	191980	640	757	-	-	4.8	2.9
RHS 80×40×4	CF-4	-	-	-	-	-	-	-
RHS 80×40×4	TC	213850	831	959	962	26	4.4	4.0

Table 4: Weighted average tensile flat material properties

Cross-section	E (N/mm^2)	$\sigma_{0.2}$ (N/mm^2)	$\sigma_{1.0}$ (N/mm^2)	σ_u (N/mm^2)	ε_f %	Compound R-O coefficients n	$n'_{0.2,1.0}$
SHS 100×100×4	198771	586	632	761	47	9.0	2.8
SHS 80×80×4	199864	679	736	773	42	6.5	4.2
SHS 60×60×3	209797	755	819	839	44	6.0	4.3
RHS 80×40×4	199500	734	785	817	50	10.1	3.4

Table 5: Weighted average compressive flat material properties

Cross-section	E (N/mm^2)	$\sigma_{0.2}$ (N/mm^2)	$\sigma_{1.0}$ (N/mm^2)	Compound R-O coefficients n	$n'_{0.2,1.0}$
SHS 100×100×4	198238	560	642	8.3	2.6
SHS 80×80×4	197185	657	770	4.7	2.6
SHS 60×60×3	206430	711	845	5.0	2.7
RHS 80×40×4	203964	607	734	4.6	2.9

Table 6: Comparison of experimental results with mill certificates

Cross-section	Tensile tests $\sigma_{0.2}$ / $\sigma_{0.2,mill}$	$\sigma_{1.0}$/ $\sigma_{1.0,mill}$	σ_u / $\sigma_{u,mill}$	Compressive tests $\sigma_{0.2}$ / $\sigma_{0.2,mill}$	$\sigma_{1.0}$ / $\sigma_{1.0,mill}$
SHS 100×100×4	0.97	0.96	0.98	0.93	0.98
SHS 80×80×4	1.26	1.22	1.03	1.22	1.27
SHS 60×60×3	1.32	1.28	1.09	1.25	1.32
RHS 80×40×4	1.36	1.30	1.09	1.12	1.21

Table 7: Measured dimensions of bending specimens

Specimen	L (mm)	B (mm)	D (mm)	t (mm)	r_i (mm)	w_0 (mm)
100×100×4-B1	1100	103.0	102.3	3.92	3.8	0.071
100×100×4-B2	1100	102.0	102.5	3.83	3.9	0.071
80×80×4-B1	1100	80.0	79.5	3.76	3.5	0.080
80×80×4-B2	1100	80.0	79.6	3.74	4.3	0.080
60×60×3-B1	1100	60.0	60.0	3.15	2.3	0.062
60×60×3-B2	1100	60.0	60.0	3.10	2.8	0.062
80×40×4-B1	1100	39.0	80.0	3.78	3.6	0.058
80×40×4-B2	1100	39.5	80.0	3.84	3.9	0.058

Table 8: Summary of test results from 3-point bending tests

Specimen	Ultimate moment M_u (kNm)	M_u/M_{el}	M_u/M_{pl}	Rotation capacity R
100×100×4-B1	39.1	1.42	1.21	2.79
100×100×4-B2	36.1	1.35	1.15	1.29
80×80×4-B1	24.9	1.39	1.18	1.35[a]
80×80×4-B2	24.3	1.38	1.16	1.29
60×60×3-B1	12.8	1.38	1.16	1.62
60×60×3-B2	12.9	1.41	1.18	1.94
80×40×4-B1	18.3	1.63	1.26	1.82[a]
80×40×4-B2	20.5	1.80	1.39	2.02[a]

[a] Full rotation capacity not attained; R based on maximum recorded deformation

Table 9: Comparison of the in-plane bending test results with FE results for varying imperfection amplitudes

Beam specimen designation	Measured amplitude w_0		t/10		t/100		Dawson and Walker	
	FE M_u/ Test M_u	FE θ_m/ Test θ_m	FE M_u/ Test M_u	FE θ_m/ Test θ_m	FE M_u/ Test M_u	FE θ_m/ Test θ_m	FE M_u/ Test M_u	FE θ_m/ Test θ_m
100×100×4-B1	0.99	0.86	0.95	0.90	0.99	0.86	0.99	0.86
100×100×4-B2	1.02	1.01	0.99	0.90	1.03	1.01	1.01	0.90
80×80×4-B1	1.05	1.24	1.00	1.08	1.05	1.19	1.05	1.19
80×80×4-B2	1.06	1.24	1.02	1.23	1.07	1.30	1.07	1.30
60×60×3-B1	0.99	0.98	0.97	0.89	1.01	1.05	1.01	1.05
60×60×3-B2	1.00	1.01	0.97	0.88	1.00	1.04	1.00	1.01
80×40×4-B1	1.02	1.40	1.00	0.99	1.02	1.34	1.02	1.40
80×40×4-B2	0.92	1.04	0.90	0.86	0.92	1.04	0.93	1.04
Mean	1.01	1.10	0.97	0.97	1.01	1.10	1.01	1.10
COV	0.04	0.16	0.04	0.13	0.04	0.14	0.04	0.17

Table 10: Comparison of test and FE results with EN 1993-1-4, SEI/ASCE 8-02, EN 1993-1-4 with modified slenderness limits and CSM.

Section type / analysis	EN 1993-1-4		EN 1993-1-4 as modified by Gardner and Theofanous (2008)		SEI/ASCE 8-02		CSM	
	Mean	COV	Mean	COV	Mean	COV	Mean	COV
Design method / FE for SHS	0.74	0.06	0.78	0.05	0.87	0.21	0.81	0.08
Design method / FE for RHS	0.83	0.14	0.87	0.11	0.92	0.19	0.92	0.07
Design method / FE for all sections	0.79	0.12	0.83	0.10	0.89	0.15	0.86	0.10
Design method / Test	0.72	0.06	0.80	0.08	0.82	0.07	0.86	0.06

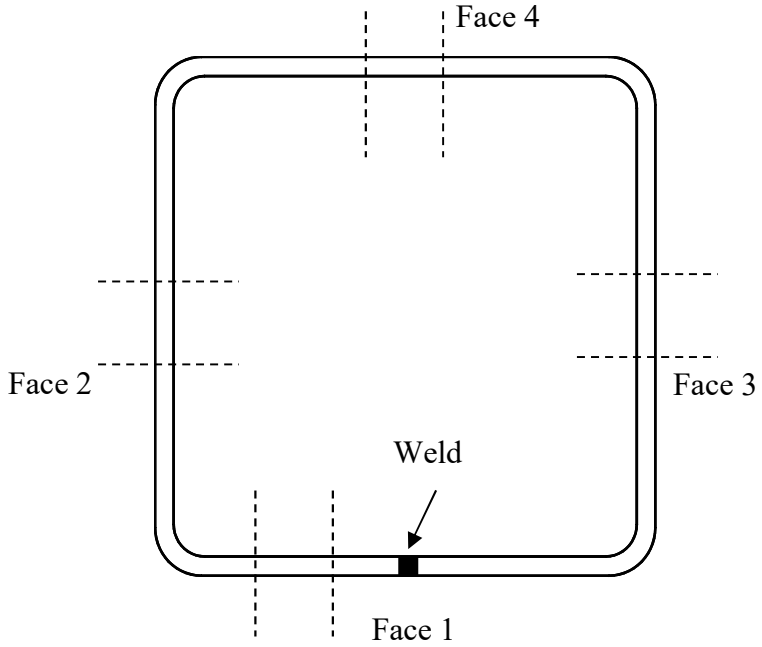

Fig. 1: Face labelling convention.

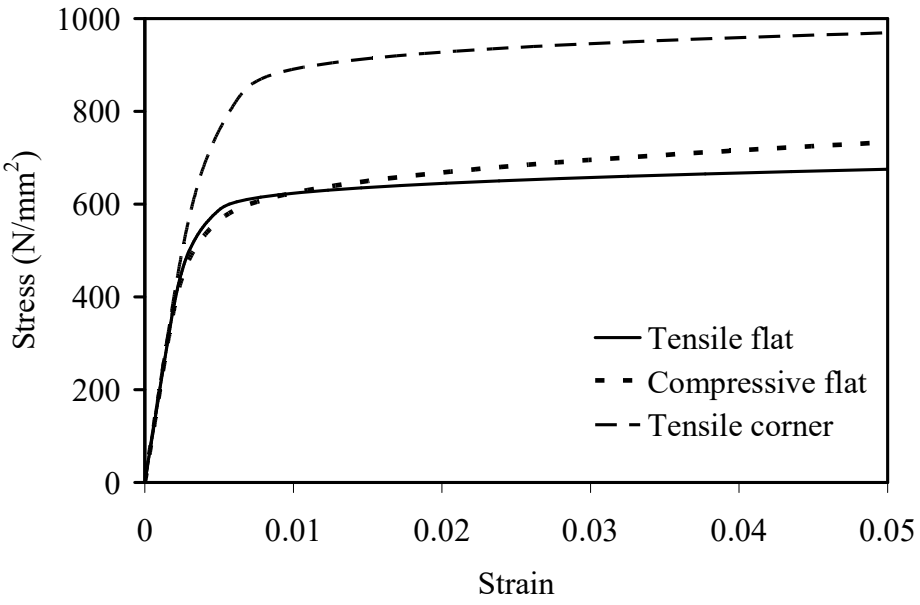

Fig. 2: Stress-strain curves for flat tensile, flat compressive and corner tensile material extracted from SHS100×100×4.

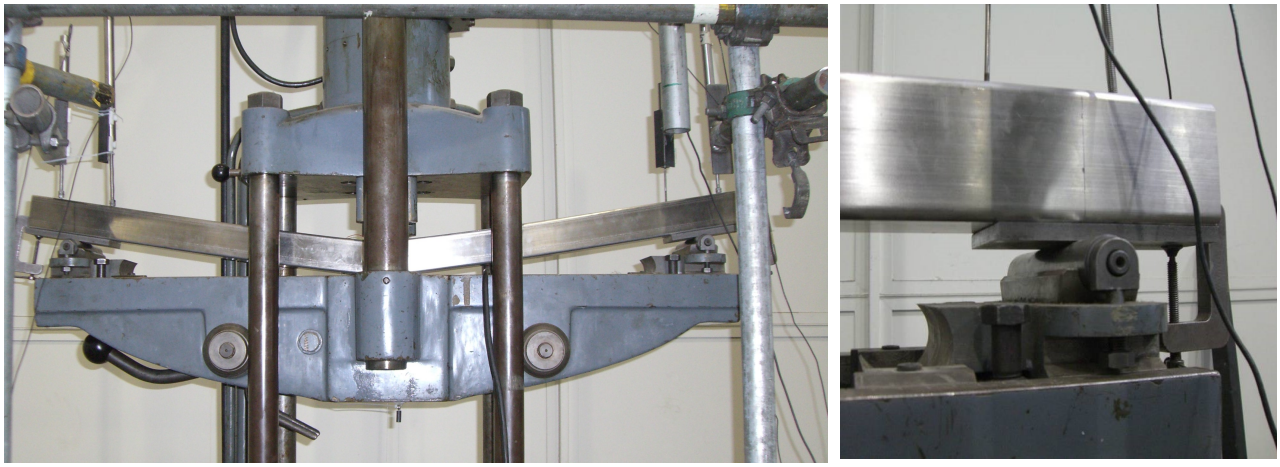

(a) Overall setup (b) Support detail

Fig. 3: Three-point bending tests.

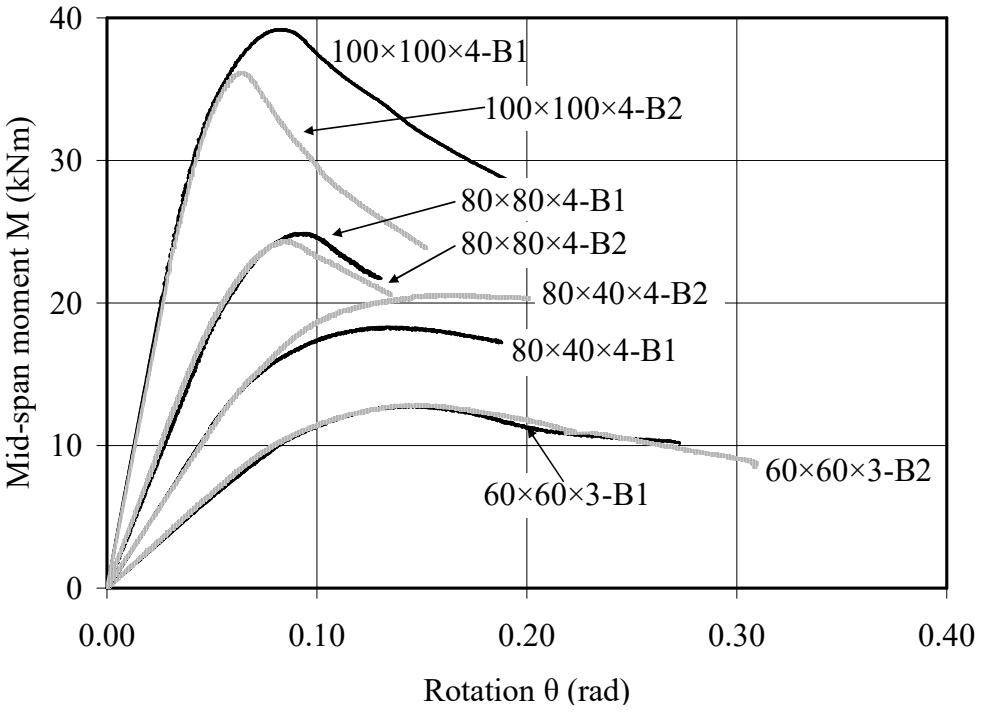

Fig. 4: Moment-rotation responses of specimens.

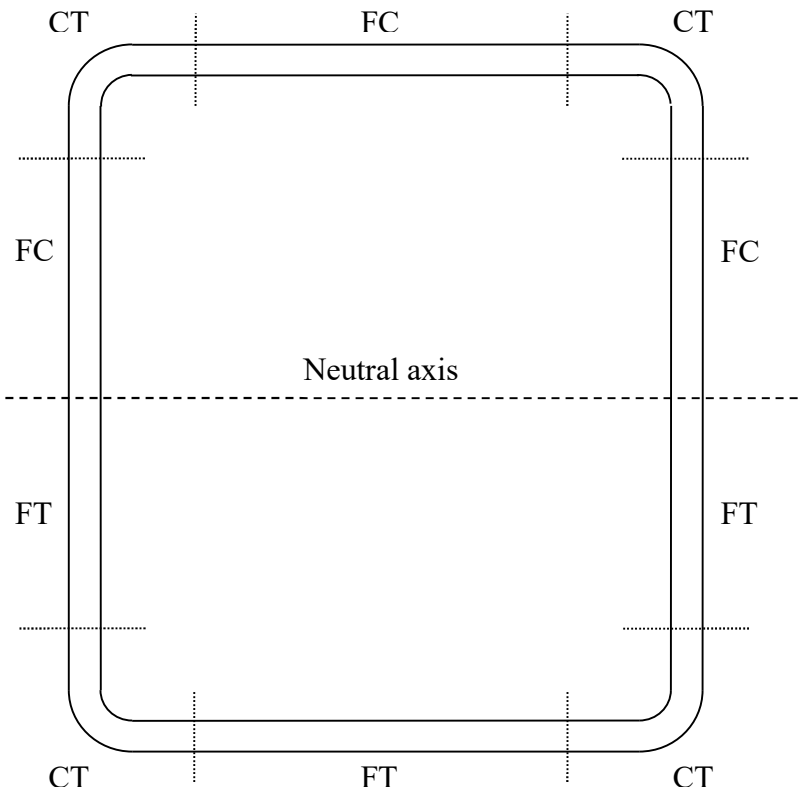

Fig. 5: Material properties assigned to the various parts of the cross-sections.

Fig. 6: Experimental and numerical failure modes for SHS 60×60×3-B2.

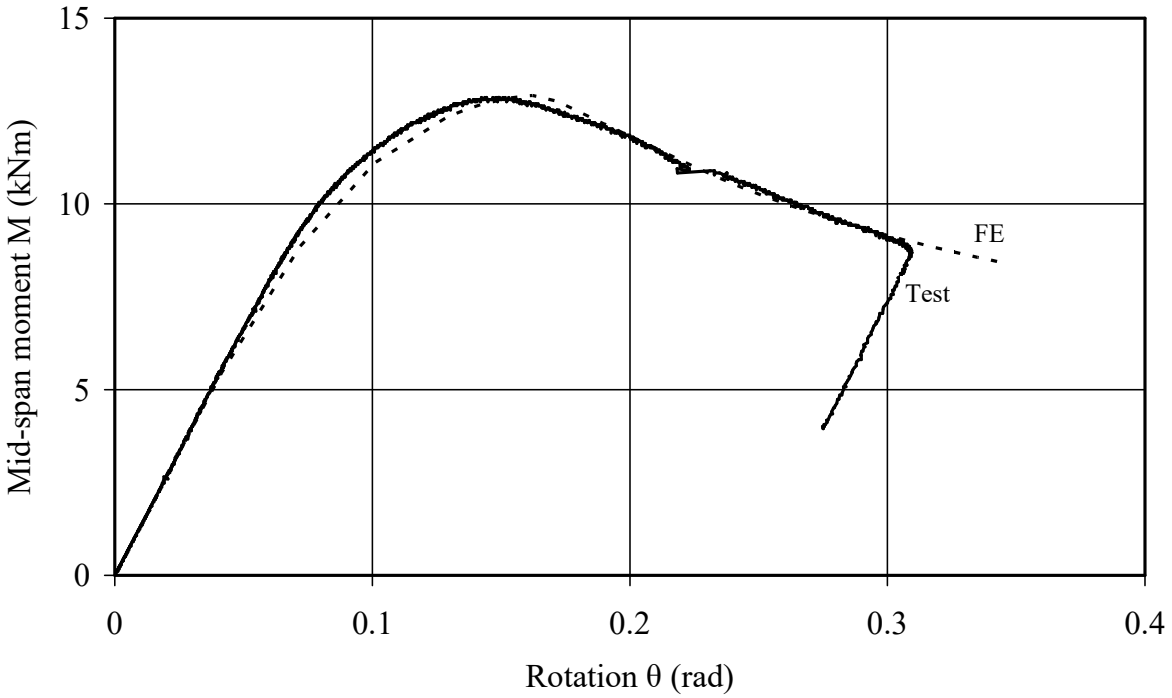

Fig. 7: Experimental and numerical moment-rotation curves for 60×60×3-B2.

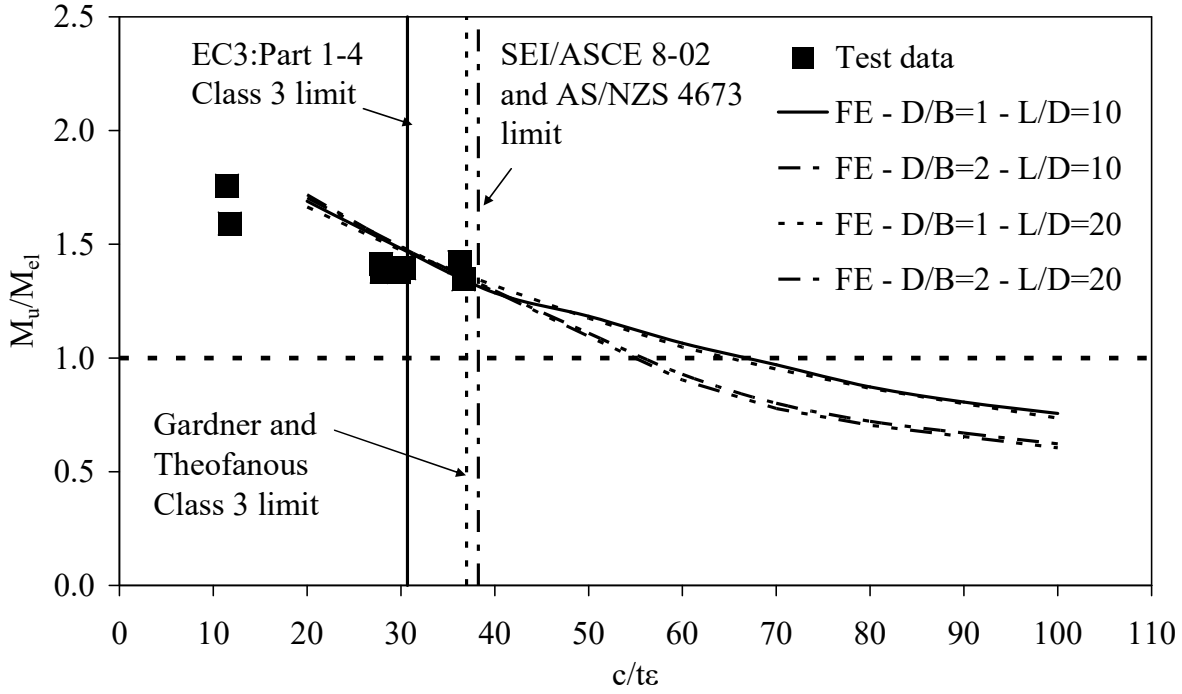

Fig. 8: Assessment of codified slenderness limits for fully effective sections (Class 3).

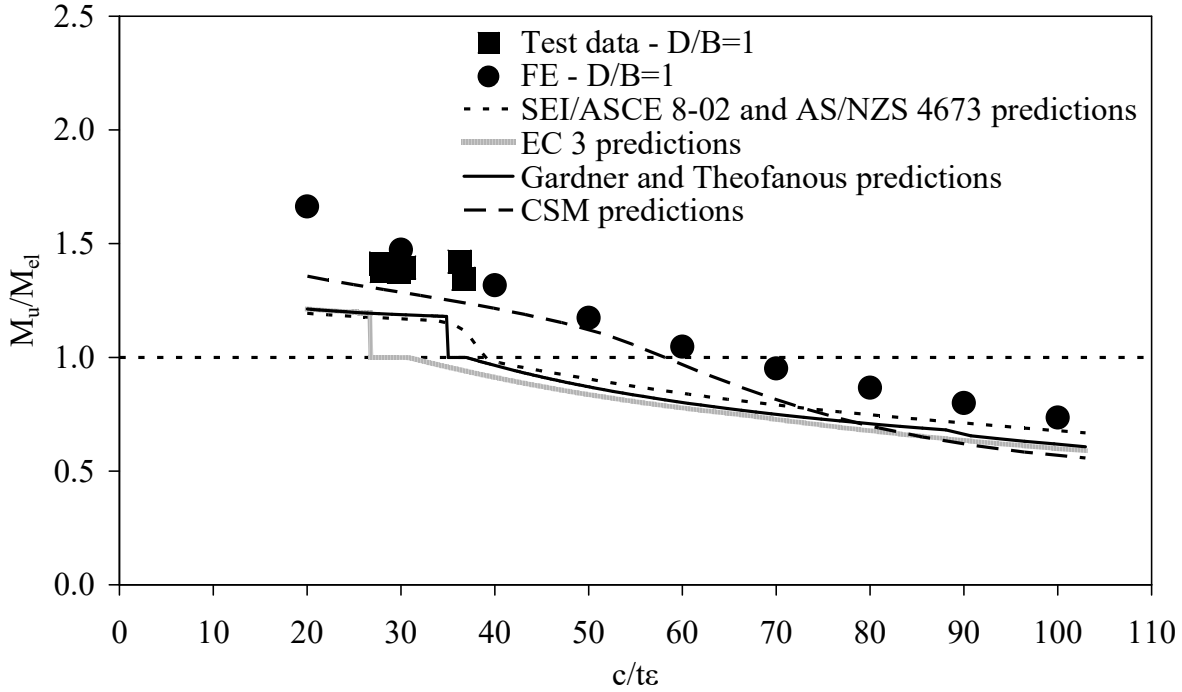

Fig. 9: Assessment of design methods for SHS (H/B=1).

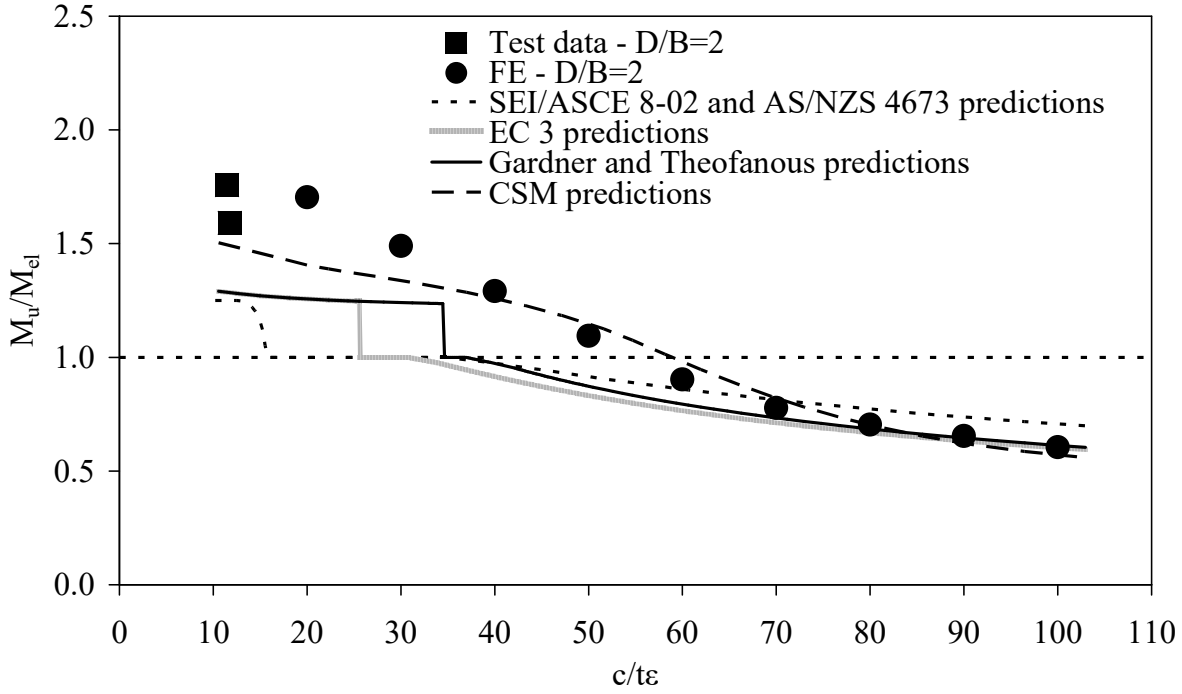

Fig. 10: Assessment of design methods for RHS (H/B=2).

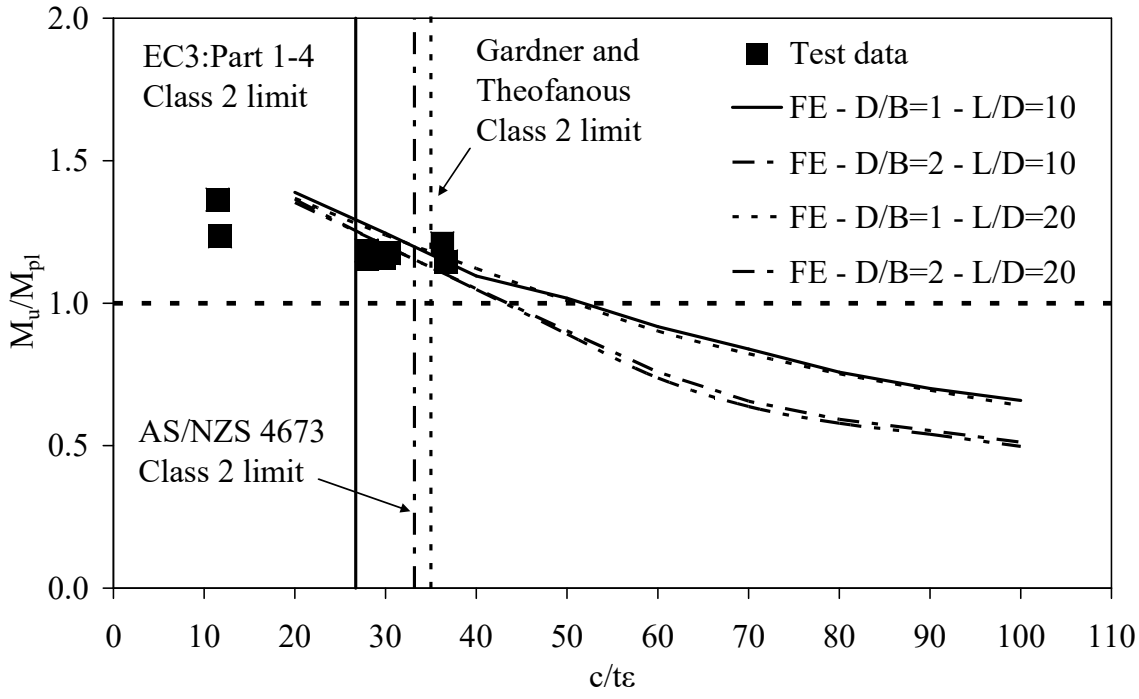

Fig. 11: Assessment of slenderness limits for compact (Class 2) sections.

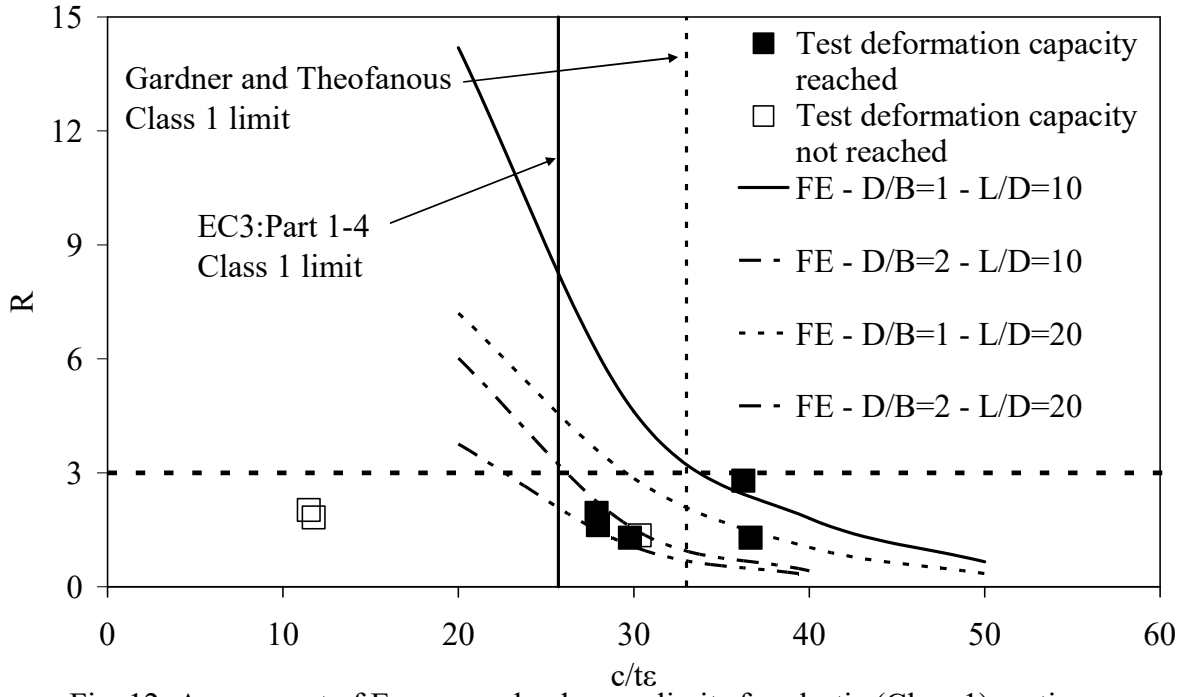

Fig. 12: Assessment of European slenderness limits for plastic (Class 1) sections.

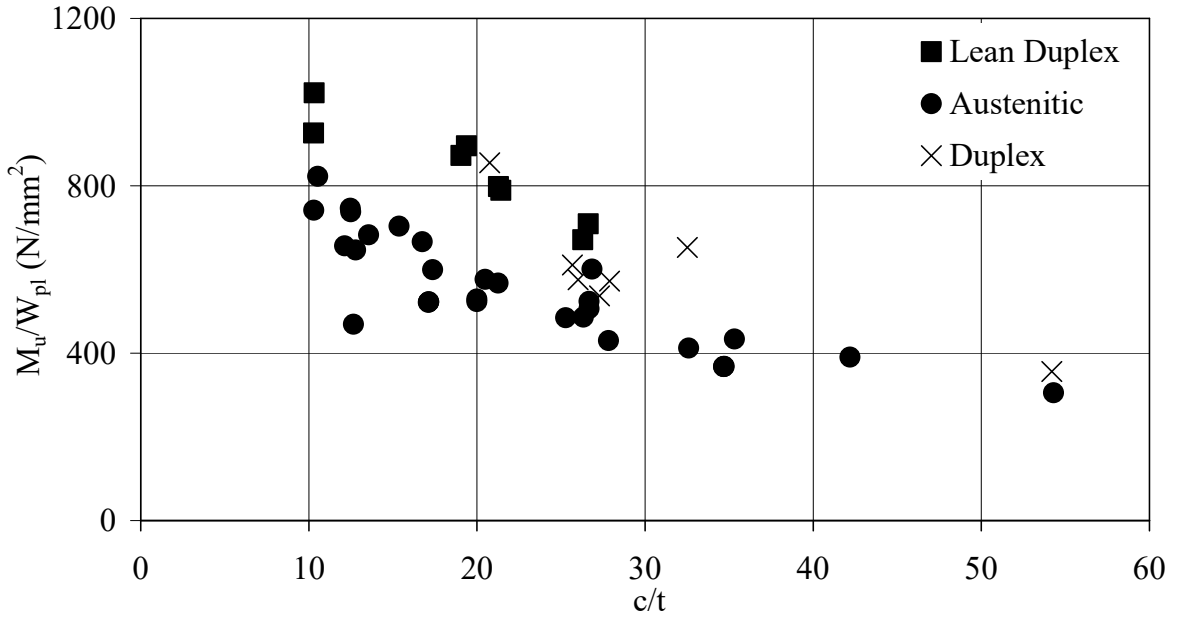

Fig. 13: Performance of SHS and RHS beams made of various grades of stainless steel.